THE JOURNAL OF PHYSICAL CHEMISTRY C

Article

pubs.acs.org/JPCC

Photon Up-Conversion with Lanthanide-Doped Oxide Particles for Solar H_2 Generation

Francisco Gonell,[†,∥] Marta Haro,[‡,∥] Rafael S. Sánchez,[‡] Patricia Negro,[‡] Iván Mora-Seró,[‡] Juan Bisquert,[‡,§] Beatriz Julián-López,*[,†] and Sixto Gimenez*[,‡]

[†]Multifunctional Materials Group, Departament de Química Inorgànica i Orgànica and [‡]Photovoltaics and Optoelectronic Devices Group, Departament de Física, Universitat Jaume I, 12071 Castelló, Spain

[§]Department of Chemistry, Faculty of Science, King Abdulaziz University, Jeddah, Saudi Arabia

Supporting Information

ABSTRACT: Up-conversion (UC) of infrared (IR) photons into visible radiation constitutes a promising strategy to enhance the light harvesting efficiency of photovoltaic and photoelectrochemical devices. In the present study, we integrate Er^{3+}/Yb^{3+}-codoped yttrium oxide (Y_2O_3) submicrometric particles with outstanding up-conversion properties into mesoporous titanium oxide (TiO_2) structures sensitized with cadmium selenide (CdSe) for solar hydrogen generation. We demonstrate that the incorporation of these up-converting particles (UCP) leads to effective H_2 generation with IR photons. Moreover, based on the analysis of the emission lifetimes, we show that the optical interaction between the emitting UCPs and the CdSe absorber occurs via a radiative emission−reabsorption process. The low cost and toxicity and excellent chemical and thermal stability of our UC phosphors allow envisaging them as real candidates for the new generation of long-term photoelectrochemical devices for solar H_2 generation.

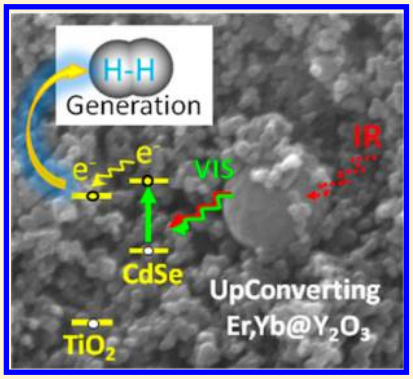

INTRODUCTION

Solar energy conversion constitutes one of the most important scientific and technological targets of the 21st century to ensure energy supply on the terawatt scale.[1,2] Remarkable progress has been achieved by third-generation photoelectrochemical and photovoltaic devices in terms of efficiency versus cost, but further optimization of their optical and electronic properties is needed for a real technological deployment.[3] One of the major drawbacks is the energy loss associated with the nonabsorbed sub-bandgap photons.[4] Consequently, different fascinating strategies, such as intermediate bandgap,[5] and spectral converters[6,7] have been attempted with the aim of optimizing their light harvesting efficiency. In this context, the use of lanthanide up-converting (UC) phosphors, which are able to transform infrared photons into visible radiation,[6,8] opens new exciting opportunities to develop more efficient devices.[4,9,10] The most studied UC systems to date involve lanthanide (Yb^{3+}, Er^{3+}, Tm^{3+}) doped fluoride materials. Among them, hexagonal (β-) phase $NaYF_4$ codoped with Yb^{3+}/Er^{3+} ions is known to be the most efficient converter due to its low phonon energy that suppresses nonradiative multiphonon relaxations.[11,12] The integration of fluoride nanocrystals in energy conversion devices for multiple applications (photovoltaics,[13] photoelectrochemistry,[10] photocatalysis,[14,15] etc.) has been recently addressed. However, fluoride materials have limited chemical and thermal stability and high costs mainly related to their complex synthetic pathways and the specific procedures for the safe use of some fluoride reagents. In contrast, metal oxides represent an exciting alternative as cheap up-converters. Despite the fact that the oxide derivatives are less efficient than their fluoride counterparts, their structural, morphological, and optical properties can be enhanced and easily tuned through stoichiometry and controlled synthetic pathways. In particular, Y_2O_3 is one of the most important oxide phosphors and has been investigated thoroughly owing to its high photoluminescence efficiency. Herein, we report for the first time the integration of Er^{3+}/Yb^{3+}-codoped yttrium oxide (Y_2O_3) submicrometric particles with outstanding UC properties into heterostructured TiO_2/CdSe photoanodes for solar hydrogen generation. The choice of yttrium oxide as host lattice for the active ions is mainly related to its low phonon energy (300−380 cm^{-1}) compared to other oxides.[16−18] Additionally, it shows a broad transparency range (0.2−8 μm), high refractive index (>1.9), large band gap (5.8 eV), excellent physical and chemical stability, and ease to be doped with rare earth ions.[19] We have particularly focused on the use of *Soft Chemistry* techniques to prepare monodisperse, crystalline, and spherical red/green nanophosphors, able to remain homogeneously distributed in mesoporous nanoparticulated films and showing a low density of surface defects, which is a key factor to enhance the optical efficiency.[20]

We demonstrate that the incorporation of Er^{3+}/Yb^{3+}:Y_2O_3 crystals into heterostructured TiO_2/CdSe photoanodes leads to the effective H_2 generation with NIR photons. Furthermore,

Received: April 16, 2014
Revised: May 3, 2014
Published: May 5, 2014

dx.doi.org/10.1021/jp503743e | J. Phys. Chem. C 2014, 118, 11279−11284

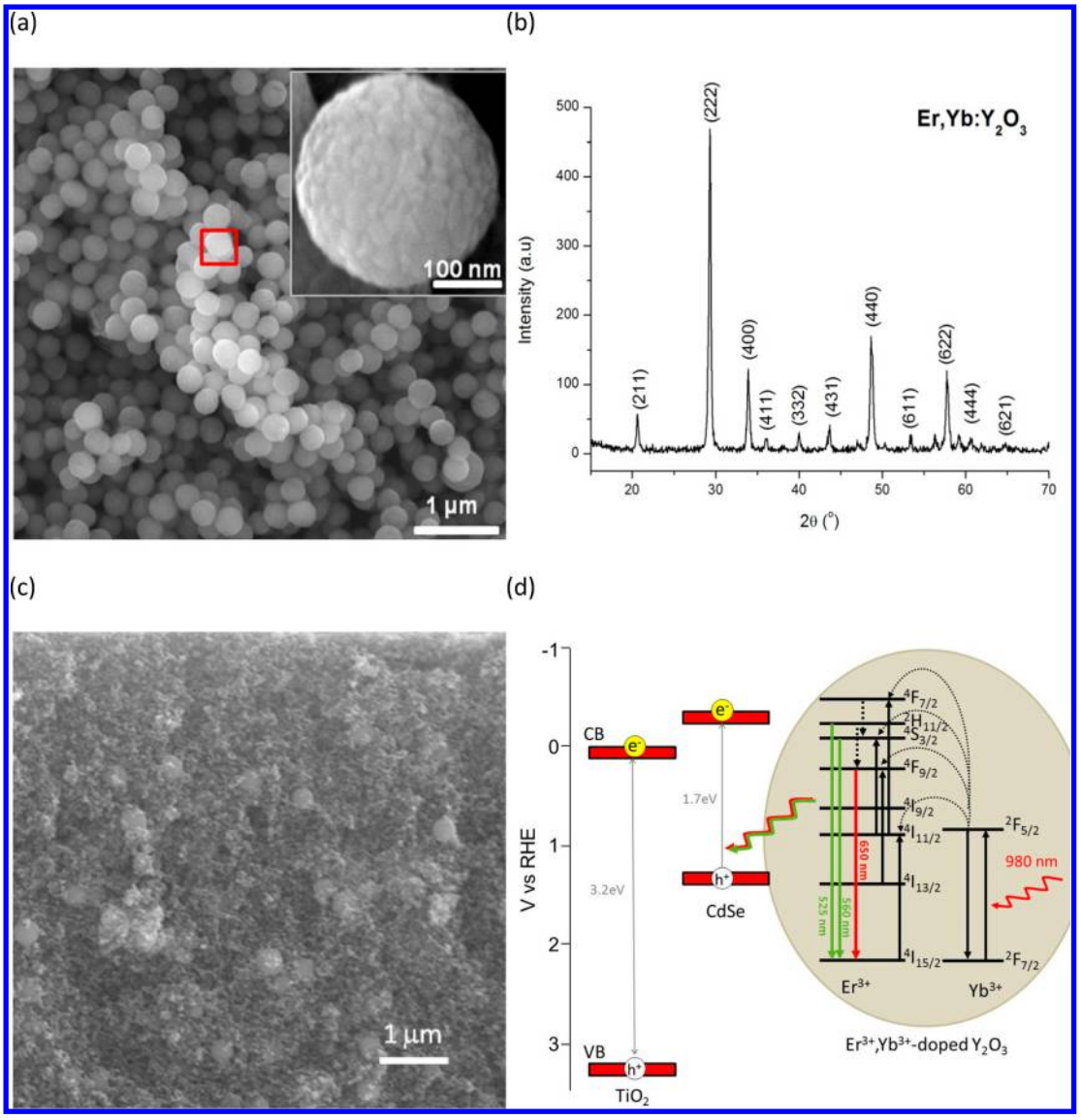

Figure 1. (a) SEM micrograph of the UCPs. The squared area is magnified at the inset showing the spherical morphology of the particles. (b) XRD spectrum of the UCPs showing its high crystallinity and single-phase structure corresponding to the cubic Y_2O_3 phase. (c) Representative cross-sectional view of the TiO_2/UCPs mesoporous films showing the good dispersion of UCPs within the mesoporous TiO_2 structure. (d) Energy diagram for the TiO_2/UCPs−CdSe photoanode and detail of the up-conversion mechanism within the UCPs.

the low cost and excellent chemical and thermal stability of these phosphors allow one to envisage them as real candidates for the new generation of long-term photoelectrochemical devices for solar H_2 generation.

EXPERIMENTAL METHOD

Synthesis of Up-Converting Particles (UCPs). Uniform size Er,Yb-doped Y_2O_3 submicrometric particles were synthesized by a homogeneous precipitation method. The stoichiometric amount of $Y(NO_3)_3{\cdot}6H_2O$, $Yb(NO_3)_3{\cdot}5H_2O$, and $Er(NO_3)_3{\cdot}5H_2O$ (all 99.9% from Alfa-Aesar) reagents to prepare $Er_{0.04}Yb_{0.1}Y_{1.86}O_3$ were dissolved in 500 mL of Milli-Q ultrapure water with a total concentration of 0.015 M. Then, the solution was heated at 80 °C and 0.25 mol of urea was added; the suspension was stirred for 6 h at this temperature. Subsequently, the turbid suspension was filtered and washed. Finally the sample was dried at 100 °C overnight and annealed at 800 °C for 2 h at a heating rate of 5 °C·min^{-1} in a muffle furnace (air atmosphere).

Preparation of TiO_2/UCPs Electrodes. The mesoporous TiO_2 paste was synthesized from commercial 20 nm TiO_2 nanoparticles (P25, Degussa) following a reported method.[21] The up-conversion particles were added in the first step of the synthesis at 20 wt %. The TiO_2/UCPs paste was deposited on FTO (SnO_2:F, TEC 15) substrates by screen printing and subsequently sintered at 450 °C for 30 min. Prior to deposition, the FTO substrates were immersed into a 40 mM titanium chloride tetrahydrofuran complex for 30 min at 70 °C and heated at 400 °C on a hot plate to form a compact layer of TiO_2. The thickness of the electrodes was ∼12 μm as measured by a contact profilometer (Dektak, Veeco).

The as-prepared mesoporous TiO_2/UCPs electrodes were sensitized with CdSe, by the successive ionic layer adsorption and reaction (SILAR) method.[22,23] The electrodes were successively immersed in two different ethanolic solutions for 30 s each, consisting of 0.03 M $Cd(NO_3)_2$ and 0.03 M Se^{2-} respectively. The process was carried out inside a glovebox under N_2 atmosphere, to prevent oxidation of the Se^{2-}

dx.doi.org/10.1021/jp503743e | J. Phys. Chem. C 2014, 118, 11279−11284

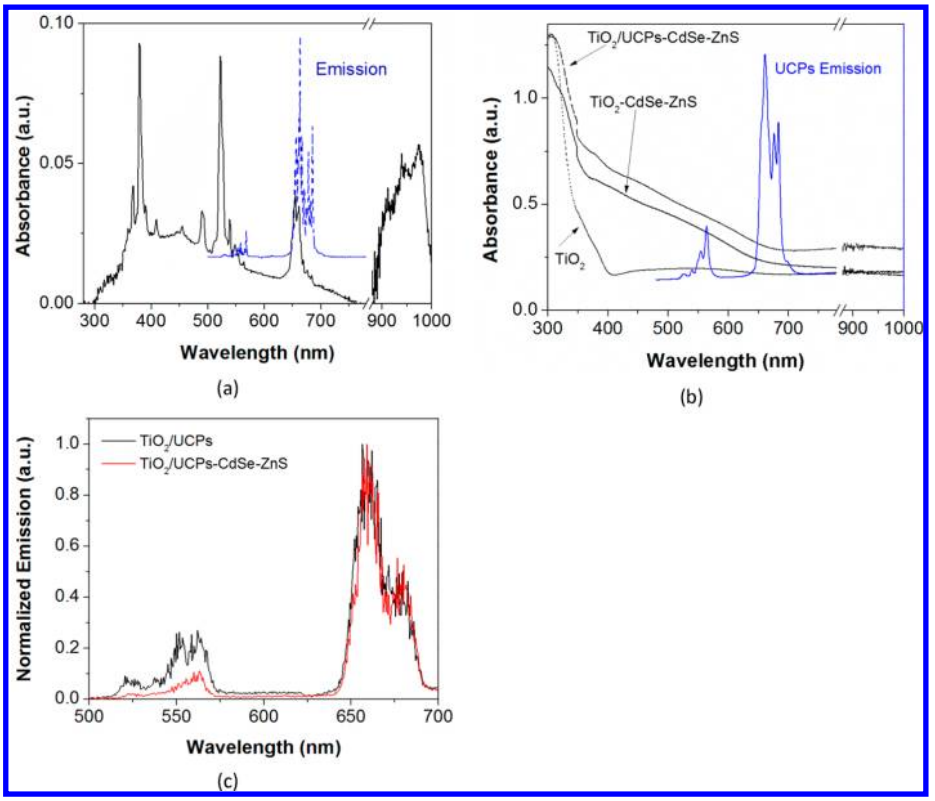

Figure 2. (a) Absorption (solid line) and emission (dashed line) (λ_{exc}: 980 nm) spectra of the UCPs. (b) Absorption spectra of the TiO_2−CdSe heterostructured photoanodes with and without the presence of the UCPs together with the emission spectrum of the UCPs. The excitation wavelength for the emission spectra was λ_{exc} = 980 nm. (c) Normalized PL emission of the UCPs embedded in CdSe sensitized and bare TiO_2 mesoporous photoanodes, showing decreased green emission at CdSe from the emitted radiation of the UCPs.

precursor. Following each immersion, rinsing and drying were undertaken using pure ethanol and N_2 gun, respectively. All these steps constitute one SILAR cycle, and a total of four cycles were carried out. All the samples analyzed in this study have been coated with a ZnS layer, after CdSe sensitization, by two SILAR cycles, each cycle consisting of alternatively dipping into 0.1 M $Zn(CH_3COO)_2$ and 0.1 M Na_2S solutions for 1 min/dip, rinsing with Milli-Q ultrapure water between dips. This ZnS treatment has demonstrated to increase both the photocurrent and stability of quantum dot sensitized solar cells based on chalcogenide materials due to a significant reduction of the recombination process of electrons in the TiO_2 with accepting species in the electrolyte as well as photocorrosion of the quantum dots.[24,25]

Characterization Techniques. Structural characterization was performed by a JEOL JEM-3100F field emission scanning electron microscope (FEG-SEM). The crystallographic structure of the up-converting particles was tested by X-ray diffraction (Siemens D5000 diffractometer with Cu Kα radiation). The transmittance (T) and diffuse reflectance (R) spectra of the UCPs and the thin films were recorded between 200 and 1100 nm by a Cary 5000 Varian spectrophotometer with an integrating $BaSO_4$ sphere. The absorbance (A) was calculated according to the equation $A = -\log(T + R)$. The steady state and time-resolved photoluminescence measurements were carried out using a Nd:YAG pulsed laser (pulse duration 4−6 ns, pulse frequency 10 Hz), model Brilliant (Quantel), coupled to an optical parametric oscillator (OPO), model Vibrant (Opotek), as excitation light source (980 nm, 2 mJ/pulse). The output signal was collected into an electronically tunable monochromator, model SpectraPro-2300i (Acton Research Corporation), coupled to a photodiode with a photomultiplier tube, model H7732−10 (Hamamatsu), and the signal was monitored using a digital oscilloscope, model TDS5000B (Tektronix). The transient PL decays were fitted to a biexponential ($y = y_0 + A_1e^{-x/\tau_1} + A_2e^{-x/\tau_2}$) function. The error intervals for the measured lifetimes were obtained from testing at least three identical samples.

Photoelectrochemical measurements were performed in a three-electrode configuration using a graphite bar as counter electrode (Sigma-Aldrich, 100 mesh) and 0.25:0.35 M NaS_2:$NaSO_3$ aqueous solution as electrolyte to prevent photocorrosion of the CdSe QDs (pH 12.7). Electrochemical measurements were referred to the reversible hydrogen electrode (RHE) by the equation $V_{RHE} = V_{Ag/AgCl} + 0.197 + 0.059 \cdot pH$. The electrodes were illuminated by a monochromatic 980 nm laser with 1500 mW/cm^2 power. The electrode illuminated area was 0.026 cm^2.

■ RESULTS AND DISCUSSION

The as-synthesized Er^{3+}/Yb^{3+}:Y_2O_3 up-converting submicrometric particles (UCPs) exhibit spherical morphology and around 300 nm diameter as shown in Figure 1a. The size distribution of the particles was measured by dynamic light scattering, and an average size of (292 ± 30) nm was obtained; see Supporting Information, Figure SI1. XRD analysis clearly shows the peaks associated with cubic yttria (JCPDS 71-0049) slightly shifted toward higher $2\theta^\circ$ in good correspondence with a solid solution in which yttrium ions are partially substituted by the smaller Er^{3+} and Yb^{3+} ions into the host lattice (effective radii in a sixfold coordination:Y^{3+} 104 pm, Yb^{3+} 101 pm, and Er^{3+} 103 pm); see Figure 1b. The chemical composition is also

dx.doi.org/10.1021/jp503743e | J. Phys. Chem. C 2014, 118, 11279−11284

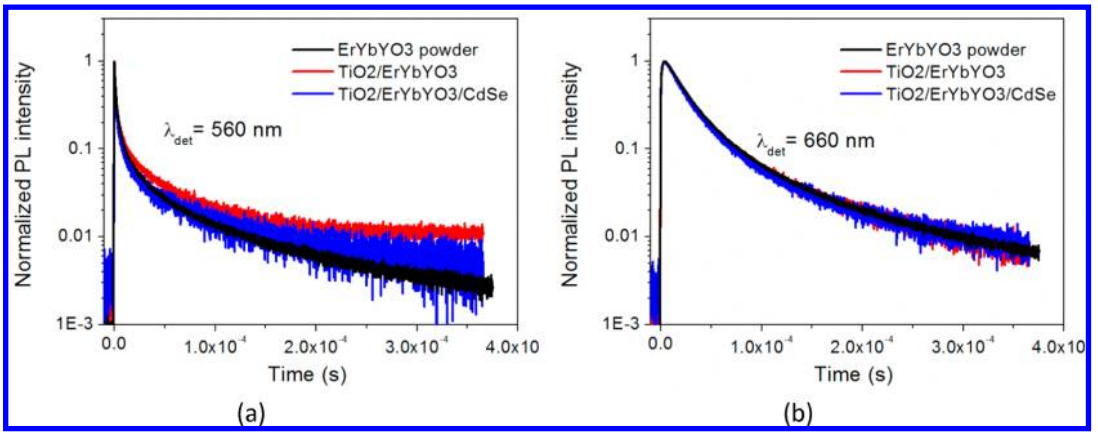

Figure 3. Decay curves recorded at the $^4S_{3/2}$ (560 nm, green emission) (a) and $^4F_{9/2}$ (660 nm, red emission) (b) Er^{3+} emitting levels upon 980 nm excitation for the bare UCPs and the TiO_2/UCPs electrodes before and after CdSe sensitization.

validated by EDS measurements (see Supporting Information, Figure SI2).

The absorbance spectrum of the Er^{3+}/Yb^{3+}:Y_2O_3 crystals presents different absorption bands in the visible region corresponding to the characteristic intraconfigurational f−f transitions from Er^{3+} ions (see Figure 2a). The broader band around 980 nm reflects the overlap of the energy levels from Er^{3+} ($^4I_{11/2}$) and Yb^{3+} ($^2F_{5/2}$) ions. Thus, upon excitation at 980 nm, the UCPs exhibit emission lines in the green ($^2H_{11/2} \rightarrow {}^4I_{15/2}$, 525 nm; $^4S_{3/2} \rightarrow {}^4I_{15/2}$, 560 nm) and red ($^4F_{9/2} \rightarrow {}^4I_{15/2}$, 660 nm) spectral regions. It is well-known that the relative intensity of both emissions depends on the concentration of the active ion (erbium) and the sensitizer (ytterbium) in the host matrix. In our case (2% Er, 5% Yb in Y_2O_3), the red emission is enhanced due to a cross-relaxation between $^2H_{11/2} \rightarrow {}^4I_{9/2}$ and $^4I_{15/2} \rightarrow {}^4I_{13/2}$, transitions.[26]

In a second step, the UCPs were incorporated into the nanoparticulated TiO_2 paste, which was deposited onto FTO conductive substrates by screen-printing. A good dispersion of the yttrium oxide phosphors and TiO_2 nanoparticles in the TiO_2/UCPs electrodes was observed from scanning electron microscopy (Figure 1c). The electrodes were further sensitized with CdSe through a SILAR method in order to make them photoactive in the visible region. A ZnS layer was added both to protect the CdSe quantum dots from photocorrosion and to enhance photocurrents by minimizing electron recombination at the TiO_2/electrolyte interface.[24,25] An accurate control of both synthetic steps was necessary to spatially arrange the different active elements in the whole system to make possible the energy connection between the UC emitting phosphor and the CdSe absorber material. Figure 1d illustrates the optical pathway of the IR photons up-converted by the Er/Yb Y_2O_3 crystals and the energetic alignment of TiO_2 and CdSe, which controls the electronic flux in the heterostructured photoanode.

Figure 2b shows the absorption spectrum of the TiO_2/UCPs−CdSe−ZnS film revealing that the heterostructures absorb light up to 670 nm. The presence of the UCPs introduces some light scattering compared to the pure TiO_2−CdSe−ZnS electrode, which is beneficial for enhanced optical absorption at the photoanode. On the other hand, negligible absorption from lanthanide f−f transitions is detected. The most interesting point here is the overlap between the green emission band from UCPs and the CdSe absorption. Indeed, we have selected the Er^{3+}/Yb^{3+} up-conversion system with two emission bands (green and red). The up-converted photons emitted around 550 nm can be directly absorbed by CdSe. The red emission is used as a reference to study the optoelectronic processes, since it is not influenced by the presence of the CdSe absorber. Therefore, according to the energy diagram in Figure 1d, we can speculate that upon IR illumination (980 nm), the up-converted photons emitted by the Er,Yb−Y_2O_3 particles will be reabsorbed by CdSe, and subsequently, the photogenerated electrons at CdSe can be injected into TiO_2, where they are transported to the contact. On the other hand, the photogenerated holes are scavenged by the reduced species of the electrolyte.

The UC properties of the electrodes before and after CdSe sensitization are shown in Figure 2c. From the emission spectra (λ_{exc} = 980 nm, normalized at the wavelength of the maximum emission), it is straightforward that red emission still dominates over the green one, indicating that the optical properties of the up-converting phosphors are preserved in the final electrodes. However, a notable decrease of the green emission intensity was detected due to the presence of CdSe nanoparticles around the phosphors. This spectral change was further investigated through time-resolved measurements. The fluorescence dynamic curves of the $^4F_{9/2} \rightarrow {}^4I_{15/2}$ (660 nm, red) and $^4S_{3/2} \rightarrow {}^4I_{15/2}$ (560 nm, green) Er^{3+} emission bands were obtained upon 980 nm excitation (see Figure 3). Lifetime values were extracted from fitting the relaxation curves to a second-order exponential function and are presented in Table 1. The curves for the time-resolved luminescence of the Er,Yb−Y_2O_3 particles

Table 1. Lifetime Values Extracted from Time-Resolved Luminescence Curves at the $^4S_{3/2}$ (560 nm, Green Emission) and $^4F_{9/2}$ (660 nm, Red Emission) Er^{3+} Emitting Levels upon 980 nm Excitation for the Bare UCPs and the TiO_2/UCPs Electrodes before and after CdSe Sensitization

sample	τ_1 (μs)[a] green emission	τ_2 (μs)[a] green emission	τ_1 (μs)[a] red emission	τ_2 (μs)[a] red emission
Er,Yb−Y_2O_3 NPs	1.8 ± 0.2	25.1 ± 1.6	19.8 ± 1.4	76.0 ± 6.4
TiO_2/UCPs	1.4 ± 0.2	28.2 ± 1.6	18.7 ± 1.4	70.3 ± 6.4
TiO_2/UCPs-CdSe	1.4 ± 0.2	25.8 ± 1.6	17.2 ± 1.4	63.2 ± 6.4

[a]The relaxation curves for both the red and green emission do not fit to a single-exponential function but a second-order exponential function; therefore, two lifetimes values for short (τ_1) and long (τ_2) relaxation contributions are included.

dx.doi.org/10.1021/jp503743e | J. Phys. Chem. C 2014, 118, 11279−11284

exhibit two contributions, probably due to the different optical behavior of the lanthanide ions located in defect coordination sites at the surface (short lifetime values) from those located in the core of the particles (with long lifetime). The lifetime values are slightly longer than those reported for this phosphor (around 25 and 5 μs for the red $^4F_{9/2} \rightarrow {}^4I_{15/2}$ and green $^4S_{3/2} \rightarrow {}^4I_{15/2}$ emissions, respectively).[27] The nonsingle exponential behavior of both transitions has been associated with a quenching effect due to $Er^{3+} \rightarrow Yb^{3+}$ back-transfer characteristic of this up-converter Er–Yb system.[28] The lifetimes do not significantly change when the UCPs are incorporated into the mesoporous TiO_2 films and further sensitized with CdSe. This fact reveals that optical interaction between the emitting UCPs and the CdSe absorber occurs via a *radiative emission–reabsorption* process, and nonradiative energy transfer mechanisms from the excited Er^{3+} moieties to the ground state of the CdSe are subsequently ruled out. Moreover, lifetimes of the red and green emissions were also obtained for the TiO_2/UCPs–CdSe–ZnS film as a function of the laser power (from 5 to 45 mW), but no significant changes were detected (Suporting Information Figure SI3). This indicates that the optical mechanism remains unaltered within this range of laser power, which can be of interest for efficient and tunable up-conversion electrochemical devices.

When the semiconductor material (CdSe) and the up-converting phosphor possess similar size, efficient energy transfer through a Forster resonance (FRET) mechanism has been identified within the heterostructure.[29,30] These studies used fluoride-based systems, which show higher up-conversion efficiencies at nanometric size due to their low phonon energy. In contrast, our oxide-based systems (with higher phonon energy) require larger size for comparable up-conversion efficiency. We believe that the large size difference between the CdSe absorber and the UCPs in our study precludes this mechanism.

Figure 4 shows the photocurrent for H_2 generation for both TiO_2–UCPs and reference TiO_2-sensitized heterostructures upon monochromatic illumination at λ = 980 nm, where CdSe absorption is negligible. In fact, the reference TiO_2-based heterostructure shows a very low photocurrent under IR illumination, ~0.1 μA·cm^{-2}, which can be due to either marginal absorption at CdSe by traps at the band gap or to sample heating effects. In contrast, the photocurrent obtained when UCPs are embedded into the mesoporous TiO_2 film is practically 1 order of magnitude higher, confirming the validity of our up-converting scheme and harnessing IR photons for H_2 generation. We also estimated the external quantum efficiency (EQE) at 980 nm, and the obtained result was 3.75 × 10^{-4} %. We note that the modest photocurrents and EQEs, in terms of absolute values, obtained in the present study have to be considered as a proof of concept. However, they are significantly higher (normalized to the power of the incident monochromatic light) compared to other values reported on previous studies demonstrating up-conversion for water photo-oxidation with fluoride-based up-converters ($NaYF_4$:Yb,Er), which are significantly more efficient, 150 nA·cm^{-2} and 1.24 × 10^{-4} %.[10] Furthermore, we underline the excellent stability of our heterostructured photoanode, with no significant performance loss after 1 h chronoamperometric measurement; see Figure 4.These results are even more significant taking into account that the addition of UCPs is detrimental for the electronic properties of the mesoporous TiO_2 films. We have characterized the electrochemical properties of both TiO_2 and TiO_2/UCPs electrodes (Supporting Information Figures SI4 and SI5), observing that the nonconducting UCPs decrease the effective TiO_2 cross section for charge transport, and consequently decrease the conductivity.[31]

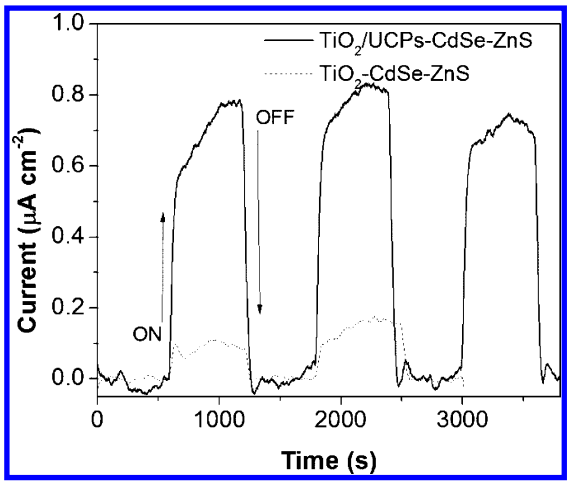

Figure 4. Photocurrent at 0 V vs Ag/AgCl (0.946 vs RHE) for TiO_2 (ref) and TiO_2/UCPs with CdSe quantum dots upon illumination with monochromatic 980 nm light (incident power 1500 mW·cm^{-2}).

CONCLUSIONS

Summarizing, we demonstrate that the incorporation of up-converting Er,Yb-codoped Y_2O_3 submicrometric particles into TiO_2/CdSe heterostructured photoanodes leads to the effective harnessing of IR photons for solar H_2 generation. We show that the up-converted photons by the phosphors are reabsorbed by the CdSe sensitizer and no energy transfer from the Er^{3+} excited state to the ground state of CdSe takes place. At this stage, the process is not efficient enough for real technological deployment, and further optimization is required. However, these results constitute an important milestone for the development of low-cost, easy-to-prepare, stable, and efficient photoelectrochemical devices for solar fuel production.

ASSOCIATED CONTENT

Supporting Information

Size distribution and chemical composition of $Er_{0.04}Yb_{0.1}Y_{1.86}O_3$ UCPs, lifetimes of emission as a function of laser power, and impedance spectroscopy analyses of the up-converting heterostructured photoelectrodes. This material is available free of charge via the Internet at http://pubs.acs.org.

AUTHOR INFORMATION

Corresponding Authors

*E-mail: julian@uji.es.
*E-mail: sjulia@fca.uji.es.

Author Contributions

‖F.G. and M.H. contributed equally to this work.

Notes

The authors declare no competing financial interest.

ACKNOWLEDGMENTS

The authors are thankful for financial support from Ministerio de Economia y Competitividad and Ministerio de Educación y Cultura (MAT2011-27008 project and AP2010-2748 PhD grant, respectively) and Jaume I University (P1 1B2010-36 and

P1·1B2011-50 projects). SCIC from Jaume I University is also acknowledged for instrumental facilities.

REFERENCES

(1) Lewis, N. S.; Nocera, D. G. Powering the Planet: Chemical Challenges in Solar Energy Utilization. *Proc. Natl. Acad. Sci. U.S.A.* **2006**, *103*, 15729−15735.

(2) Maeda, K.; Domen, K. Photocatalytic Water Splitting: Recent Progress and Future Challenges. *J. Phys. Chem. Lett.* **2010**, *1*, 2655−2661.

(3) Walter, M. G.; Warren, E. L.; McKone, J. R.; Boettcher, S. W.; Mi, Q.; Santori, E. A.; Lewis, N. S. Solar Water Splitting Cells. *Chem. Rev.* **2010**, *110*, 6446−6473.

(4) van Sark, W.; de Wild, J.; Rath, J. K.; Meijerink, A.; Schropp, R. E. I. Upconversion in Solar Cells. *Nanoscale Res. Lett.* **2013**, *8*, 1−10.

(5) Luque, A.; Marti, A.; Stanley, C. Understanding Intermediate-Band Solar Cells. *Nat. Photonics* **2012**, *6*, 146−152.

(6) Haase, M.; Schafer, H. Upconverting Nanoparticles. *Angew. Chem., Int. Ed. Engl.* **2011**, *50*, 5808−5829.

(7) Strumpel, C.; McCann, M.; Beaucarne, G.; Arkhipov, V.; Slaoui, A.; Svrcek, V.; del Canizo, C.; Tobias, I. Modifying the Solar Spectrum to Enhance Silicon Solar Cell Efficiency—An Overview of Available Materials. *Sol. Energy Mater. Sol. Cells* **2007**, *91*, 238−249.

(8) Auzel, F. Upconversion and Anti-Stokes Processes with F and D Ions in Solids. *Chem. Rev.* **2004**, *104*, 139−173.

(9) Su, L. T.; Karuturi, S. K.; Luo, J. S.; Liu, L. J.; Liu, X. F.; Guo, J.; Sum, T. C.; Deng, R. R.; Fan, H. J.; Liu, X. G.; et al. Photon Upconversion in Hetero-Nanostructured Photoanodes for Enhanced Near-Infrared Light Harvesting. *Adv. Mater.* **2013**, *25*, 1603−1607.

(10) Zhang, M.; Lin, Y. J.; Mullen, T. J.; Lin, W. F.; Sun, L. D.; Yan, C. H.; Patten, T. E.; Wang, D. W.; Liu, G. Y. Improving Hematite's Solar Water Splitting Efficiency by Incorporating Rare-Earth Upconversion Nanomaterials. *J. Phys. Chem. Lett.* **2012**, *3*, 3188−3192.

(11) Kramer, K. W.; Biner, D.; Frei, G.; Gudel, H. U.; Hehlen, M. P.; Luthi, S. R. Hexagonal Sodium Yttrium Fluoride Based Green and Blue Emitting Upconversion Phosphors. *Chem. Mater.* **2004**, *16*, 1244−1251.

(12) Wang, F.; Liu, X. G. Upconversion Multicolor Fine-Tuning: Visible to Near-Infrared Emission from Lanthanide-Doped Na_yF_4 Nanoparticles. *J. Am. Chem. Soc.* **2008**, *130*, 5642−5643.

(13) Huang, X. Y.; Han, S. Y.; Huang, W.; Liu, X. G. Enhancing Solar Cell Efficiency: The Search for Luminescent Materials as Spectral Converters. *Chem. Soc. Rev.* **2013**, *42*, 173−201.

(14) Tang, Y. N.; Di, W. H.; Zhai, X. S.; Yang, R. Y.; Qin, W. P. NIR-Responsive Photocatalytic Activity and Mechanism of Na_yF_4:Yb,Tm@TiO_2 Core−Shell Nanoparticles. *ACS Catal.* **2013**, *3*, 405−412.

(15) Xu, D. X.; Lian, Z. W.; Fu, M. L.; Yuan, B. L.; Shi, J. W.; Cui, H. J. Advanced Near-Infrared-Driven Photocatalyst: Fabrication, Characterization, and Photocatalytic Performance of Beta-$NaYF_4$:Yb^{3+},Tm^{3+}@TiO_2 Core@Shell Microcrystals. *Appl. Catal., B* **2013**, *142*, 377−386.

(16) Capobianco, J. A.; Vetrone, F.; Boyer, J. C.; Speghini, A.; Bettinelli, M. Enhancement of Red Emission (F-4(9/2) → I-4(15/2)) via Upconversion in Bulk and Nanocrystalline Cubic Y_2O_3:Er^{3+}. *J. Phys. Chem. B* **2002**, *106*, 1181−1187.

(17) Capobianco, J. A.; Vetrone, F.; D'Alesio, T.; Tessari, G.; Speghini, A.; Bettinelli, M. Optical Spectroscopy of Nanocrystalline Cubic Y_2O_3:Er^{3+} Obtained by Combustion Synthesis. *Phys. Chem. Chem. Phys.* **2000**, *2*, 3203−3207.

(18) Tissue, B. M. Synthesis and Luminescence of Lanthanide Ions in Nanoscale Insulating Hosts. *Chem. Mater.* **1998**, *10*, 2837−2845.

(19) Korzenski, M. B.; Lecoeur, P.; Mercey, B.; Camy, P.; Doualan, J. L. Low Propagation Losses of an Er:Y_2O_3 Planar Waveguide Grown by Alternate-Target Pulsed Laser Deposition. *Appl. Phys. Lett.* **2001**, *78*, 1210−1212.

(20) Guo, H.; Qiao, Y. M. Preparation, Characterization, and Strong Upconversion of Monodisperse Y_2O_3:Er^{3+},Yb^{3+} Microspheres. *Opt. Mater.* **2009**, *31*, 583−589.

(21) Ito, S.; Chen, P.; Comte, P.; Nazeeruddin, M. K.; Liska, P.; Pechy, P.; Gratzel, M. Fabrication of Screen-Printing Pastes from TiO_2 Powders for Dye-Sensitized Solar Cells. *Prog. Photovoltaics* **2007**, *15*, 603−612.

(22) Gonzalez-Pedro, V.; Xu, X. Q.; Mora-Sero, I.; Bisquert, J. Modeling High-Efficiency Quantum Dot Sensitized Solar Cells. *ACS Nano* **2010**, *4*, 5783−5790.

(23) Lee, H. J.; Wang, M.; Chen, P.; Gamelin, D. R.; Zakeeruddin, S. M.; Grätzel, M.; Nazeeruddin, M. K. Efficient CdSe Quantum Dot-Sensitized Solar Cells Prepared by an Improved Successive Ionic Layer Adsorption and Reaction Process. *Nano Lett.* **2009**, *9*, 4221−4227.

(24) Gimenez, S.; Lana-Villarreal, T.; Gomez, R.; Agouram, S.; Munoz-Sanjose, V.; Mora-Sero, I. Determination of Limiting Factors of Photovoltaic Efficiency in Quantum Dot Sensitized Solar Cells: Correlation between Cell Performance and Structural Properties. *J. Appl. Phys.* **2010**, *108* (064310), 1−7.

(25) Braga, A.; Gimenez, S.; Concina, I.; Vomiero, A.; Mora-Sero, I. Panchromatic Sensitized Solar Cells Based on Metal Sulfide Quantum Dots Grown Directly on Nanostructured TiO_2 Electrodes. *J. Phys. Chem. Lett.* **2011**, *2*, 454−460.

(26) Patra, A.; Friend, C. S.; Kapoor, R.; Prasad, P. N. Upconversion in Er^{3+}:ZrO_2 Nanocrystals. *J. Phys. Chem. B* **2002**, *106*, 1909−1912.

(27) Vetrone, F.; Boyer, J. C.; Capobianco, J. A.; Speghini, A.; Bettinelli, M. Significance of Yb^{3+} Concentration on the Upconversion Mechanisms in Codoped Y_2O_3:Er^{3+},Yb^{3+} Nanocrystals. *J. Appl. Phys.* **2004**, *96*, 661−667.

(28) Auzel, F.; Baldacchini, G.; Laversenne, L.; Boulon, G. Radiation Trapping and Self-Quenching Analysis in Yb^{3+}, Er^{3+}, and HO^{3+} Doped Y_2O_3. *Opt. Mater.* **2003**, *24*, 103−109.

(29) Bednarkiewicz, A.; Nyk, M.; Samoc, M.; Strek, W. Up-Conversion Fret from Er^{3+}/Yb^{3+}:$NaYF_4$ Nanophosphor to CdSe Quantum Dots. *J. Phys. Chem. C* **2010**, *114*, 17535−17541.

(30) Yan, C.; Dadvand, A.; Rosei, F.; Perepichka, D. F. Near-IR Photoresponse in New Up-Converting CdSe/$NaYF_4$:Yb,Er Nano-heterostructures. *J. Am. Chem. Soc.* **2010**, *132*, 8868−8869.

(31) Fabregat-Santiago, F.; Garcia-Belmonte, G.; Mora-Seró, I.; Bisquert, J. Characterization of Nanostructured Hybrid and Organic Solar Cells by Impedance Spectroscopy. *Phys. Chem. Chem. Phys.* **2011**, *13*, 9083−9118.